

2 Interannual variability of stratospheric and tropospheric ozone 3 determined from satellite measurements

4 Jack Fishman, John K. Creilson,¹ and Amy E. Wozniak¹

5 NASA Langley Research Center, Hampton, Virginia, USA

6 Paul J. Crutzen²

7 Max-Planck-Institute for Chemistry, Mainz, Germany

8 Received 10 February 2005; revised 3 May 2005; accepted 3 August 2005; published XX Month 2005.

9 [1] Long-term satellite records have been used in previous studies to examine both trends
10 and interannual variability (IAV) of ozone in the stratosphere. In this study, we use
11 satellite measurements to produce long-term records of both tropospheric and stratospheric
12 ozone and we examine the IAV of these data sets. Our analysis of the stratospheric
13 component of these observations is consistent with previous findings for total ozone that
14 show a strong correlation with the quasi-biennial oscillation (QBO) at low latitudes. For
15 tropospheric ozone, we find that there are strong regional enhancements due to in situ
16 generation from large emissions. The IAV of some of these regional enhancements, on the
17 other hand, are strongly correlated with the phase of El Niño–Southern Oscillation
18 (ENSO) and are consistent with our understanding of how regions of subsidence are more
19 conducive to the in situ production of ozone pollution. The insight gained from this study
20 will hopefully provide a better understanding between prevailing meteorological
21 conditions and the evolution of widespread ozone episodes on shorter timescales with the
22 eventual goal of producing an air quality forecasting capability so that exposure of the
23 human population to elevated levels of ozone can be reduced.

24 **Citation:** Fishman, J., J. K. Creilson, A. E. Wozniak, and P. J. Crutzen (2005), Interannual variability of stratospheric and
25 tropospheric ozone determined from satellite measurements, *J. Geophys. Res.*, 110, DXXXXX, doi:10.1029/2005JD005868.

27 1. Introduction

28 [2] Elevated ozone concentrations produced as a result of
29 fossil and domestic fuel combustion contribute to a number
30 of human ailments such as respiratory diseases [*Spektor et*
31 *al.*, 1988; *Koren et al.*, 1989; *Lippmann and Schlesinger*,
32 2000]. Furthermore, the recent study by *Bell et al.* [2004]
33 shows that moderate increases in tropospheric ozone con-
34 centrations of only 10 ppbv lead to increased rates of
35 mortality in U.S. metropolitan areas that translate to nearly
36 4000 premature deaths annually. Other studies have also
37 shown that elevated surface ozone concentrations have
38 deleterious effects on both crop production [*Heck et al.*,
39 1983] and specific types of plants [*Skelly*, 2000] at con-
40 centrations well below the current NAAQS standard of 80 ppbv.
41 On a global scale, surface ozone concentrations have
42 increased significantly during the past century [*Volz and*
43 *Kley*, 1988; *Staehelin et al.*, 1994] because of increased
44 anthropogenic emissions from industrial and agricultural
45 processes. The concurrent increased emissions of nitrogen

oxides and hydrocarbons in the presence of sunlight are the 46
primary factors leading to these higher concentrations of 47
ozone. 48

[3] The long-term data record of tropospheric ozone 49
residual (TOR) distributions ([http://asd-www.larc.nasa.gov/](http://asd-www.larc.nasa.gov/TOR/data.html) 50
TOR/data.html) has used concurrent measurements from the 51
Total Ozone Mapping Spectrometer (TOMS) and Solar 52
Backscattered Ultraviolet (SBUV) instruments to develop 53
a quasi-global tropospheric ozone climatology [*Fishman et* 54
al., 2003]. This climatology shows significant regional 55
enhancements of ozone pollution resulting from the release 56
of copious emissions from regionally industrialized areas in 57
the Northern Hemisphere and widespread biomass burning 58
in the tropics. In addition to the climatological and seasonal 59
distributions discussed by *Fishman et al.* [2003], this data 60
record spans more than two decades (1979–2000) yielding 61
nearly 17 years of monthly averaged depictions. Within this 62
record, there is significant interannual variability (IAV) of 63
elevated pollution in certain regions. Because of the unique 64
length and data density of this tropospheric trace gas 65
database, it is possible, for the first time, to examine the 66
IAV of the TOR and to see if this IAV can be correlated with 67
other well-known IAV parameters: The quasi-biennial oscil- 68
lation (QBO) and the El Niño–Southern Oscillation 69
(ENSO). 70

[4] Another objective of this study is to examine a 71
complimentary integrated data set that is also derived from 72

¹Also at Science Applications International Corporation (SAIC),
Hampton, Virginia, USA.

²Also at Scripps Institute of Oceanography, La Jolla, California, USA.

Region	Lat	Monthly SCO Correlations											
		Jan	Feb	Mar	Apr	May	Jun	Jul	Aug	Sep	Oct	Nov	Dec
	N=>	18	18	17	18	17	17	17	18	18	18	17	17
West Africa (20W-30E)	15-20N	-.23	-.34	-.37	-.48	-.39	-.12	.07	-.20	-.20	-.20	-.10	-.17
	10-15N	.18	.03	-.06	-.09	.12	.27	.44	.09	.10	.05	.16	.13
	5-10N	.55	.46	.40	.31	.53	.57	.71	.53	.56	.54	.55	.52
	E-5N	.64	.63	.67	.60	.73	.73	.82	.73	.74	.72	.70	.65
	E-5S	.53	.65	.68	.66	.74	.73	.83	.70	.64	.63	.70	.54
	5-10S	.36	.56	.56	.57	.62	.49	.59	.34	.26	.33	.56	.27
	10-15S	.11	.37	.31	.25	.18	.02	-.15	-.49	-.35	-.37	-.10	-.14
	15-20S	-.10	.13	.01	-.16	-.31	-.31	-.55	-.78	-.68	-.65	-.51	-.38
India (60-120E)	15-20N	-.28	-.17	-.40	-.45	-.48	-.27	.11	-.04	.04	.15	-.08	-.31
	10-15N	.21	.23	-.02	-.17	.05	.18	.38	.21	.36	.40	.23	-.08
	5-10N	.60	.64	.49	.41	.52	.52	.64	.53	.67	.70	.73	.44
	E-5N	.65	.69	.67	.69	.67	.63	.78	.72	.80	.79	.87	.65
	E-5S	.62	.66	.68	.73	.71	.65	.78	.73	.79	.74	.83	.58
	5-10S	.54	.59	.57	.66	.62	.35	.50	.35	.47	.48	.67	.34
	10-15S	.30	.41	.27	.34	.22	-.21	-.33	-.48	-.42	-.26	-.04	-.27
	15-20S	.02	.20	-.06	-.13	-.23	-.45	-.64	-.69	-.68	-.56	-.57	-.49
Pacific (160-100W)	15-20N	-.34	-.19	-.37	-.36	-.53	-.17	.02	-.09	-.17	-.03	-.06	-.18
	10-15N	-.02	.08	-.03	-.11	-.13	.17	.32	.17	.12	.23	.27	.11
	5-10N	.34	.44	.40	.28	.30	.49	.65	.51	.47	.55	.69	.54
	E-5N	.53	.63	.65	.57	.56	.69	.79	.67	.59	.65	.79	.65
	E-5S	.50	.64	.73	.67	.63	.72	.78	.66	.54	.58	.71	.89
	5-10S	.29	.49	.63	.56	.53	.55	.45	.35	.21	.26	.42	.34
	10-15S	.02	.25	.38	.19	.19	.10	-.35	-.49	-.51	-.43	-.29	-.09
	15-20S	-.14	.08	.15	-.22	-.25	-.32	-.71	-.80	-.80	-.69	-.63	-.33

Key (all correlations in bold are significant to at least the .05 level):

Positive Correlation and level of significance of at least .01:
 Positive Correlation and level of significance of at least .05:
 Negative Correlation and level of significance of at least .01:
 Negative Correlation and level of significance of at least .05:

Figure 1. Correlation coefficients between stratospheric column ozone (SCO) and one of the quasi-biennial oscillation (QBO) indices (wind speed at 30 hPa over Singapore), displayed as a function of month and latitude. Instead of using zonally averaged SCO quantities, these correlations have been computed for three different east-west domains: near the Prime Meridian over and south of west Africa, south of India, and over the eastern Pacific. The blue and green regions indicate strong positive correlations (generally near the equator and at all times of the year) whereas the yellow and orange regions indicate regions of anti-correlation (generally at southern subtropical latitudes during austral spring).

73 the TOR methodology applied to the TOMS and SBUV
 74 measurements. The stratospheric column ozone (SCO) is
 75 the integrated amount of ozone above the tropopause
 76 and its climatological distribution is in excellent agree-
 77 ment with a comparable quantity derived from Strato-
 78 spheric Aerosol and Gas Experiment (SAGE) profiles
 79 [Wozniak *et al.*, 2005]. Thus, in this study, we also
 80 show that the IAV of SCO is consistent with earlier
 81 studies that have examined the relationship between
 82 TOMS total ozone and the QBO, leading to an impor-
 83 tant confirmation of the use of TOR methodology to
 84 investigate IAV behavior.

85 [5] On the other hand, the regional and long-term
 86 nature of the TOR fields is a unique attribute of this
 87 data set. Whereas the QBO is observed on a significantly
 88 large spatial scale in the stratosphere, we find that some
 89 of the regions where significant air pollution is found

display IAV that is highly correlated with ENSO. Such a
 relationship may provide important insight for determin-
 ing when prolonged elevated pollution events may be
 conducive to formation, and possibly even lead to iden-
 tifying specific meteorological situations that portend
 pollution episodes.

2. Derivation of Data Set Used in this Study

[6] TOMS total ozone measurements have been available
 from several satellites since November 1978 (see <http://toms.gsfc.nasa.gov>). Nimbus-7 operated from November
 1978 through April 1993; the Earth Probe satellite operated
 at a relatively low orbit of 540 km and provided higher
 spatial resolution from July 1996 through December 1997
 and then was boosted to a higher orbit of 740 km to obtain
 complete global coverage. For the current study, Nimbus-7

105 TOMS data (Version 7) from 1979 through 1993 and Earth
 106 Probe data from 1997 through 2000 have been analyzed.
 107 Only data from the Nimbus-7 and Earth Probe have been
 108 used in this study to take advantage of the availability of the
 109 aerosol index information that is part of the correction we
 110 apply to the measurements [Torres and Bhartia, 1999;
 111 Fishman and Balok, 1999].

112 [7] The SCO is determined from SBUV profiles integrated
 113 from the tropopause to the top of the atmosphere. Before
 114 integration above the tropopause, each SBUV profile is
 115 empirically corrected so that the amount of ozone below the
 116 tropopause is set equal to the monthly climatological
 117 amount determined from the Logan [1999] analysis. This
 118 quantity is then subtracted from the SBUV total ozone
 119 column to derive the SCO [Fishman and Balok, 1999;
 120 Fishman et al., 2003]. That value (i.e., the integrated ozone
 121 amount above the tropopause derived from the SBUV
 122 measurement) is then used as input to derive a stratospheric
 123 ozone field using other such measurements over a 5-day
 124 period to determine the field for the central day. That
 125 quantity is then subtracted from the concurrent TOMS total
 126 ozone amount on the central day to calculate the TOR for
 127 this study. Tropopause height information for the current
 128 study uses gridded (2.5° latitude by 2.5° longitude) analyses
 129 provided by the National Centers for Environmental Pre-
 130 diction (NCEP). These analyses are produced every 6 hours
 131 and the value closest to the time of the SBUV observation is
 132 used in the current study. For the discussion presented in the
 133 following sections, we present monthly maps that have been
 134 derived from the TOR distribution calculated daily and then
 135 averaged over the month.

3. Stratospheric and Tropospheric IAV in the Tropics

3.1. Relationship Between Stratospheric Ozone and the QBO

140 [8] In addition to quantifying the global nature of secular
 141 trends in stratospheric ozone depletion, long-term total
 142 ozone satellite measurements (i.e., TOMS and SAGE) have
 143 been used to investigate multiyear cycles that also can be
 144 found in these data records [Bowman, 1989; Chandra and
 145 Stolarski, 1991; Tung and Yang, 1994; Kinnersley and
 146 Tung, 1998]. One of the strongest and most clear-cut signals
 147 found in these total ozone records is that of the quasi-
 148 biennial oscillation (QBO), a feature that was first observed
 149 for stratospheric equatorial winds [Reed, 1965]. The QBO
 150 is a well-documented meteorological phenomenon
 151 [Lindzen and Holton, 1968] in which the zonal winds in
 152 the lower stratosphere change direction with a periodicity
 153 of 24–30 months. In accordance with this change of wind
 154 direction, the amount of ozone in the stratosphere also
 155 changes where a strong westerly component is associated
 156 with relatively higher amounts of ozone while an easterly
 157 component is associated with relatively lower amounts. In
 158 addition, the analysis of SAGE O_3 profile data has shown
 159 that the QBO signal propagates throughout vertically
 160 within the stratosphere [Hasebe, 1996; Randel and Wu,
 161 1996].

162 [9] In this section, we examine the relationship between
 163 the stratospheric column ozone (SCO) and parameters that
 164 can be used to define QBO. Kinnersley and Tung [1998]

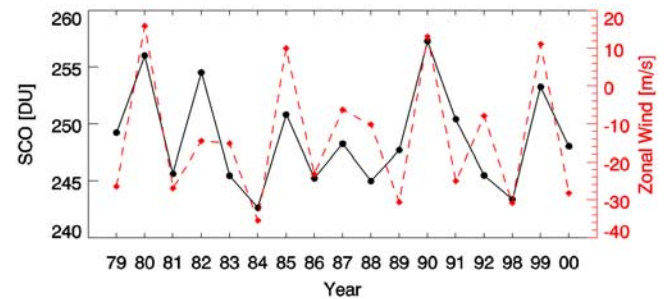


Figure 2. Solid black line showing a time series of the monthly average amount of ozone in the stratosphere (stratospheric column ozone, SCO), for June for years for which there are data between 1979 and 2000 for the equatorial region (5°N – 5°S) between 20°W and 30°E (West Africa); dashed red line shows the mean zonal for June at 30 hPa over Singapore (one index used to define the phase of the QBO). The correlation coefficient for these two variables is +0.73.

165 have provided a comprehensive analysis of the correlation
 166 between TOMS total ozone and stratospheric winds over
 167 Singapore. In Figure 1, we present a similar analysis, but
 168 instead of using complete zonal averages, we break the
 169 equatorial regimes into three regions: West Africa (20°W –
 170 30°E); India (60°E – 120°E); and Central Pacific (160°W –
 171 100°W) (QBO data courtesy of University of Washington
 172 and can be found at http://tao.atmos.washington.edu/data_sets/qbo/). Furthermore, instead of using TOMS total
 173 ozone, we use the monthly SCO values that are derived
 174 through our calculation of TOR using coincident TOMS
 175 total ozone information and profile information from SBUV
 176 measurement between 1979 and 2000. The number of
 177 monthly SCO values going into the correlation coefficient
 178 calculations is shown as the first number in each column.
 179 Our findings of the relationship between the SCO and the
 180 QBO at low latitudes are qualitatively the same as those
 181 of Kinnersley and Tung [1998] using a 13-year record of
 182 TOMS and Singapore winds from 1980–1993. In the
 183 band along the equator (5°N – 5°S), 63 of the 72 correla-
 184 tion coefficients show a level of significance of at least
 185 0.01, meaning that there is less than a 1% chance that the
 186 two sets of data are not correlated; the remainder of the
 187 correlation coefficients in these latitude bands have a
 188 level of significance of 0.05, implying that there is less
 189 than a 5% chance that the QBO and SCO values are not
 190 correlated. The monthly correlations become less positive
 191 when they are calculated farther away from the equator.
 192 Furthermore, there is an anti-correlation in the southern
 193 subtropics (15°S – 20°S) during late austral winter through
 194 austral spring (July–November). Kinnersley and Tung’s
 195 correlation analysis yielded nearly identical findings
 196 where the austral spring anti-correlation extended to
 197 southern middle and high latitudes (regions not of interest
 198 in this study). In the discussion that follows, it is
 199 significant that the IAV for the SCO data behave in a
 200 manner that is consistent with our understanding of
 201 stratospheric dynamics and that the nature of this behav-
 202 ior at low latitudes is regionally independent (as defined
 203

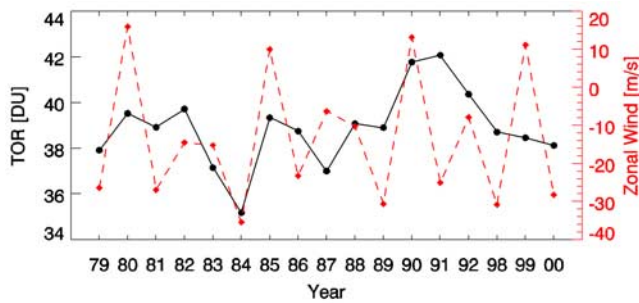


Figure 3. Average amount of tropospheric ozone for each June over the West Africa region plotted against the same QBO index as shown in Figure 2. The correlation coefficient between these two variables is 0.36, which is not significant.

204 by the three regions in Figure 1). A specific time series
 205 for the month of June is shown in Figure 2 where the
 206 SCO for the West Africa box defined in Figure 1 is
 207 plotted as a function of year against the monthly average
 208 zonal wind measured over Singapore at 30 hPa, a
 209 commonly used indicator of the phase of the QBO. The
 210 correlation coefficient of the two variables in this time
 211 series is +0.73.

212 **3.2. Interannual Variability Over West Africa**

213 [10] Although the IAV of equatorial stratospheric ozone is
 214 dominated by dynamical processes related to the QBO, the
 215 ozone distribution in the troposphere is correlated to a
 216 significantly less degree with the QBO. The plot shown in
 217 Figure 3 is similar to the one shown in Figure 2 except it
 218 shows the relationship between the June TOR over the same
 219 region over West Africa and the QBO. These two variables
 220 have a correlation coefficient of 0,36, which is not signifi-
 221 cant with this number of data points.

222 [11] ENSO indices, which consist of the Southern Oscilla-
 223 tion Index (SOI) and equatorial Pacific Ocean sea surface
 224 temperature anomalies (SSTAs), are illustrated in Figure 4

(image provided by NOAA Climate Prediction Center from 225
 their web site at <http://www.cpc.ncep.noaa.gov>). The origi- 226
 nal SOI was defined as the pressure difference between 227
 Darwin (northern Australia) and Tahiti (central equatorial 228
 Pacific) [Philander, 1990]. More recent definitions of 229
 ENSO use sea surface temperature variations in regions 230
 of the equatorial Pacific to define the strength of the phase 231
 of El Niño; specifically, these indices quantify the departure 232
 from the average temperature (sea surface temperature 233
 anomaly, SSTa) in specific regions. Region 1 + 2 is a 234
 relatively small area in the extreme eastern Pacific near the 235
 Peruvian coast, the region first recognized as changing 236
 significantly during the ENSO cycle. In more recent times, 237
 when technology developed so that more remote regions 238
 could be monitored, other larger areas of the Pacific were 239
 defined and found to be generally more impacted by the 240
 coupled ocean-atmosphere nature of the ENSO. Thus Re- 241
 gion 3 is a larger area encompassing the equatorial eastern 242
 Pacific whereas Region 4 has been defined as the box in the 243
 western/central Pacific; by convention, Region 3.4 denotes 244
 the central Pacific. For the discussion on the TOR over West 245
 Africa that follows, we will use the standard SOI index to 246
 examine the relationship between ENSO and tropospheric 247
 ozone. We will also refer to the various SSTAs in later 248
 discussions. The SCO and SOI correlation coefficient for 249
 June in this region is a statistically insignificant 0.26. 250

[12] An example of the IAV in the TOR field is clearly 251
 illustrated by the distributions shown in Figure 5 where 252
 significantly more ozone is observed during June over 253
 western Africa during 1982, a strong El Niño year, as 254
 compared to 1984, a strong La Niña year. In addition to a 255
 weaker relationship (but still sometimes significant) be- 256
 tween TOR amounts and the QBO over western Africa, 257
 we have found that the pattern of the distribution is at times 258
 highly correlated to the phase of ENSO. To define this 259
 pattern, we examine the difference in the amount of ozone 260
 north and south of the equator: $\Delta(\text{TOR}) = \text{TOR}_{0^{\circ}-5^{\circ}\text{N}} -$ 261
 $\text{TOR}_{0^{\circ}-5^{\circ}\text{S}}$. Figure 6 illustrates the strong nature of this 262
 correlation for the month of June, where $\Delta(\text{TOR})$ is com- 263
 pared with the Sea Surface Temperature Anomaly (SSTA) 264

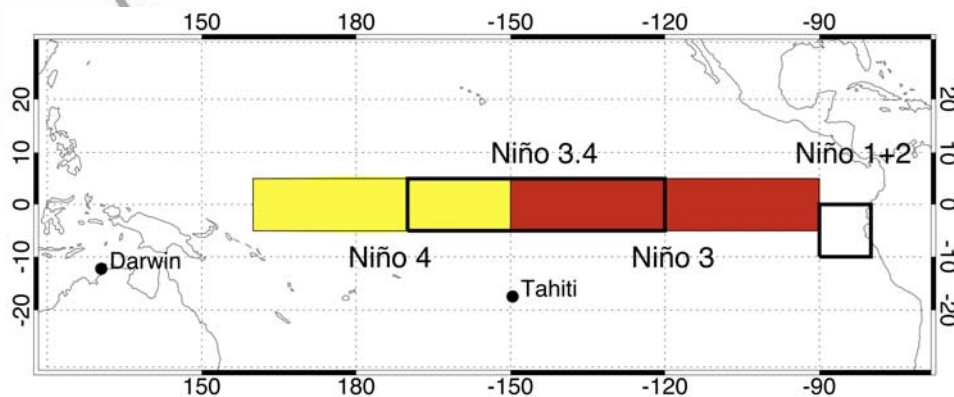


Figure 4. Graphical depiction of the Sea Surface Temperature Anomaly Regions used to define ENSO intensity: Niño region 1 + 2 is the area off the coast of Ecuador; Region 3 is the red box in the eastern Pacific; Region 4 is the yellow box in the western Pacific; Region 3.4 is the overlapping area in the central Pacific. The classic Southern Oscillation Index (SOI) is defined as the difference between the surface pressure at Darwin, Australia, and Tahiti.

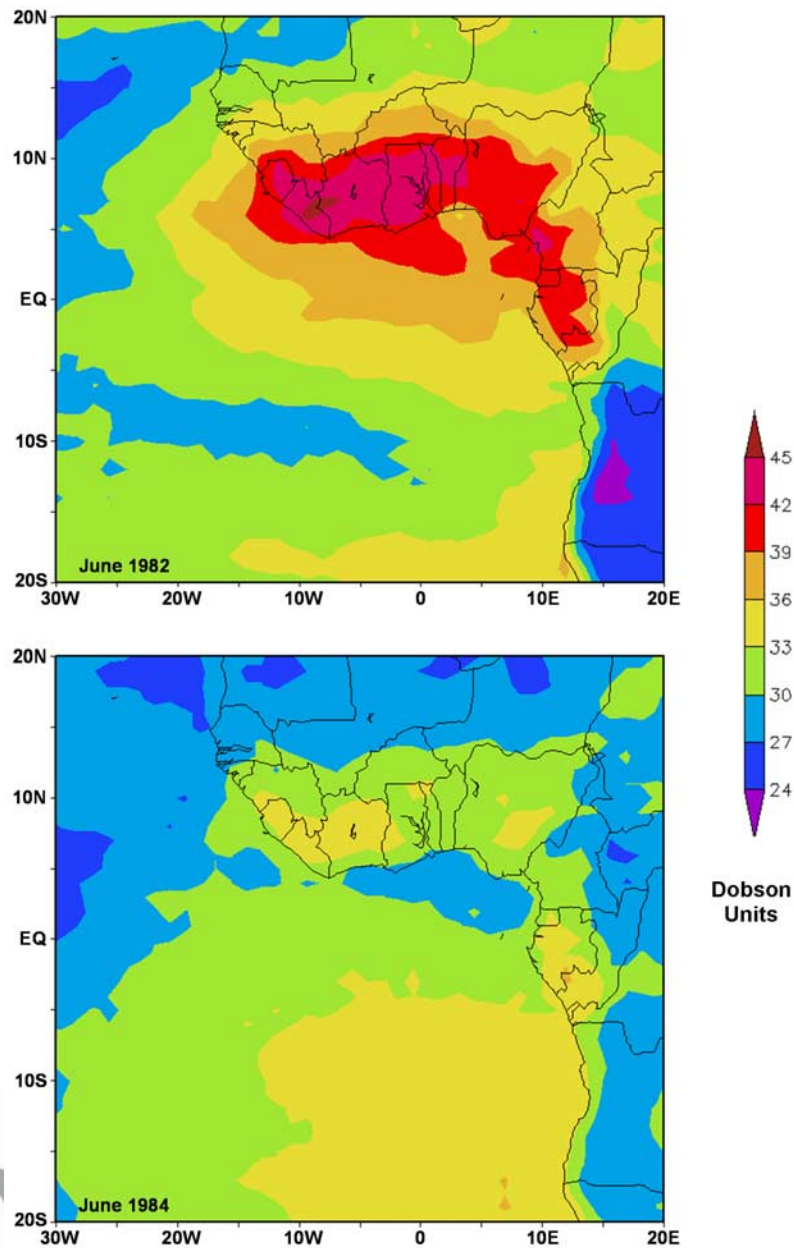


Figure 5. Depiction of the interannual variability of tropospheric ozone during June of a strong El Niño year (1982) and June of a strong La Niña year (1984).

265 observed over the west central Pacific (El Niño Region 4),
 266 where the resultant correlation coefficient for these two
 267 variables is 0.78.

268 [13] Cook [1999] investigated the meteorology over this
 269 region through an analysis of the African Easterly Jet (AEJ)
 270 and precipitation over West Africa. He found that during the
 271 summer months the climatological African Easterly Jet
 272 formed in the presence of a negative soil moisture gradient,
 273 peaking at approximately 15°N. The jet, which is typically
 274 located at ~600 hPa, is driven by the difference in strong
 275 summer insolation and dryness over Saharan Africa to the
 276 north and the wet season over West Africa and western
 277 Sahelian Africa to the south. Several studies show that
 278 anomalously drier summers are linked to a southward

279 displacement of both the Intertropical Convergence Zone
 280 (ITCZ) and the AEJ [Grist and Nicholson, 2001; Nicholson
 281 and Grist, 2003]. This southward displacement means that
 282 the precipitation processes (i.e., the West African summer
 283 monsoon) that the AEJ/ITCZ help drive also setup farther
 284 south, creating a situation where subsidence is prevalent
 285 over this region of West Africa.

286 [14] Earlier studies linked the phase of ENSO with
 287 African rainfall, through an analysis of the phase of a
 288 defined 2-year ENSO cycle and its relationship with the
 289 strength of the Atlantic and Indian Ocean SSTAs [e.g.,
 290 Nicholson and Kim, 1997]. Similarly, we find that during
 291 the summers of El Niño years (as defined by the June El
 292 Niño 4 SSTAs), the AEJ and ITCZ appear to be displaced

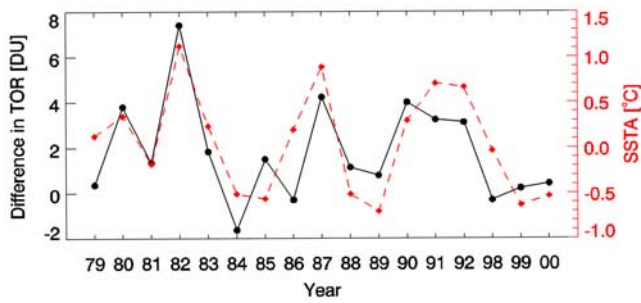


Figure 6. A measure of the North/South gradient ($TOR_{0^{\circ}-5^{\circ}N} - TOR_{0^{\circ}-5^{\circ}S}$) plotted as the black solid line; the Sea Surface Temperature Anomaly in the west/central Pacific Ocean, a measure of the phase of the ENSO, is shown by the dashed red line. The correlation coefficient between these two variables is 0.78.

293 farther south, and that vertical velocity (ω) over our West
 294 African study region is anomalously positive. Figure 7
 295 (image provided by the NOAA-CIRES Climate Diagnostics
 296 Center, Boulder Colorado from their Web site at [http://www.cdc.noaa.gov/\[Kalnay et al., 1996\]](http://www.cdc.noaa.gov/[Kalnay et al., 1996])) shows the average
 297 vertical velocity at 700 hPa over this region during the “El
 298 Niño” years (Figure 7, top) and the distribution of the
 299 correlation coefficient between ω and the SOI index over
 300 the period 1979–2000 (Figure 7, bottom). These depictions
 301 suggest that meteorological conditions during El Niño years
 302 favor strong subsidence in the lower troposphere over this
 303 region. In addition to the increased subsidence, the meteo-
 304 rological data [Kalnay et al., 1996] also clearly show that
 305 both the precipitation amounts and rate are considerably
 306 lower during the El Niño summers relative to other years.

308 [15] The presence of widespread subsidence can be con-
 309 ducive to enhanced ozone in the troposphere for several
 310 reasons. When rain is reduced, the relatively drier land and
 311 clearer skies provide more favorable conditions for wide-
 312 spread vegetation burning which can lead to larger amounts
 313 of ozone precursors being emitted. Such conditions are also
 314 conducive to more sunshine and thus ozone being generated
 315 more efficiently through enhanced photochemical activity.
 316 Last, widespread subsidence would more efficiently bring
 317 higher levels of ozone down from the upper troposphere and
 318 lower stratosphere. Unfortunately, the sources of elevated
 319 TOR values cannot be differentiated without in situ mea-
 320 surements that better define the vertical structure of ozone
 321 within the troposphere.

323 **4. IAV of Tropospheric Ozone Over Northern**
 324 **India and East China**

325 [16] The use of satellites to measure the distribution of
 326 tropospheric trace gases has provided a new appreciation for
 327 how local and regional emissions strongly influence the
 328 resultant global distribution of these trace species. The
 329 Figure 8 (top) (image courtesy Institute of Environmental
 330 Physics, University of Heidelberg, and can be found at
 331 <http://satellite.iup.uni-heidelberg.de>) shows that NO_2 emis-
 332 sions come predominately from northern temperate latitudes
 333 and to a lesser extent from tropical Africa and South
 334 America. The satellite-derived TOR product shows consid-

erably greater amounts in NH summer (Figure 8, bottom) 335
 when sunlight is sufficiently prevalent to generate ozone 336
 efficiently. Recent depictions for satellite-derived carbon 337
 monoxide distributions also show emissions emanating from 338
 regions of high anthropogenic activity and widespread tropi- 339
 cal biomass burning [Edwards et al., 2003; Frankenberg et 340
 al., 2005]. 341

[17] There have also been recent studies showing a 342
 relationship between satellite-derived tropospheric column 343
 ozone (TCO) amounts and the phase of the ENSO cycle in 344
 the tropics [Ziemke and Chandra, 2003]. In that study, they 345
 compared TCO data at two tropical locations, Tahiti and 346
 Darwin, with the difference in pressure at those two sites 347
 (the conventional definition of the Southern Oscillation 348

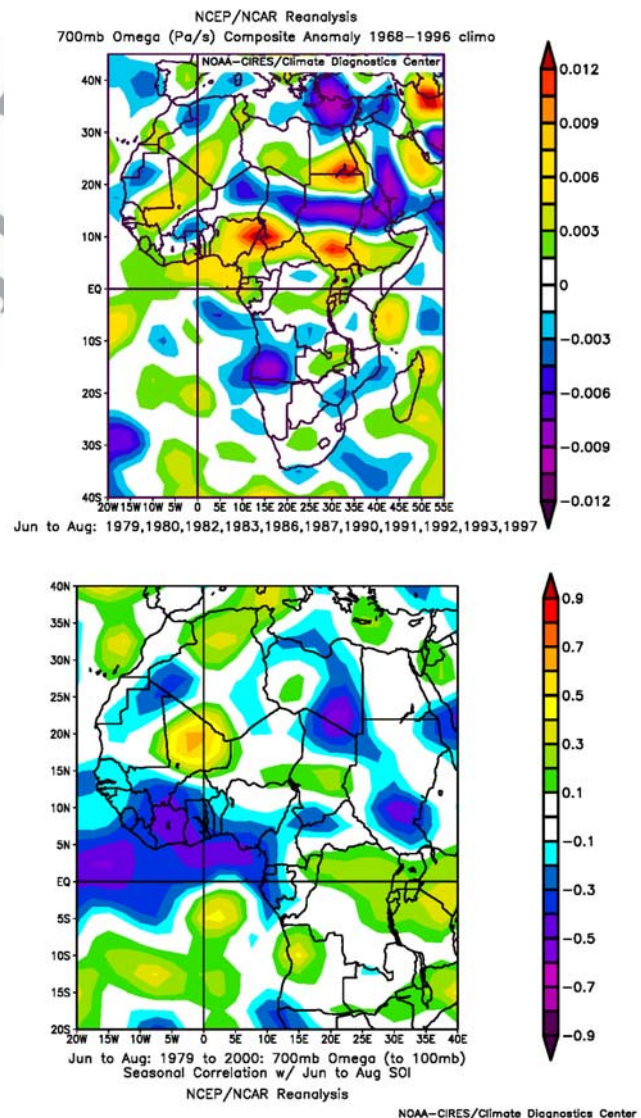


Figure 7. (top) An analysis of June–August vertical velocity, ω (omega), at 700 hPa over West Africa during El Niño years (1979, 1980, 1982, 1983, 1986, 1987, 1990, 1991, 1992, 1993, 1997). Positive ω_{700} is indicative of subsidence. (bottom) Distribution of the correlation coefficient between ω and the SOI index over Africa. Strongest correlation is found over Gulf of Guinea region.

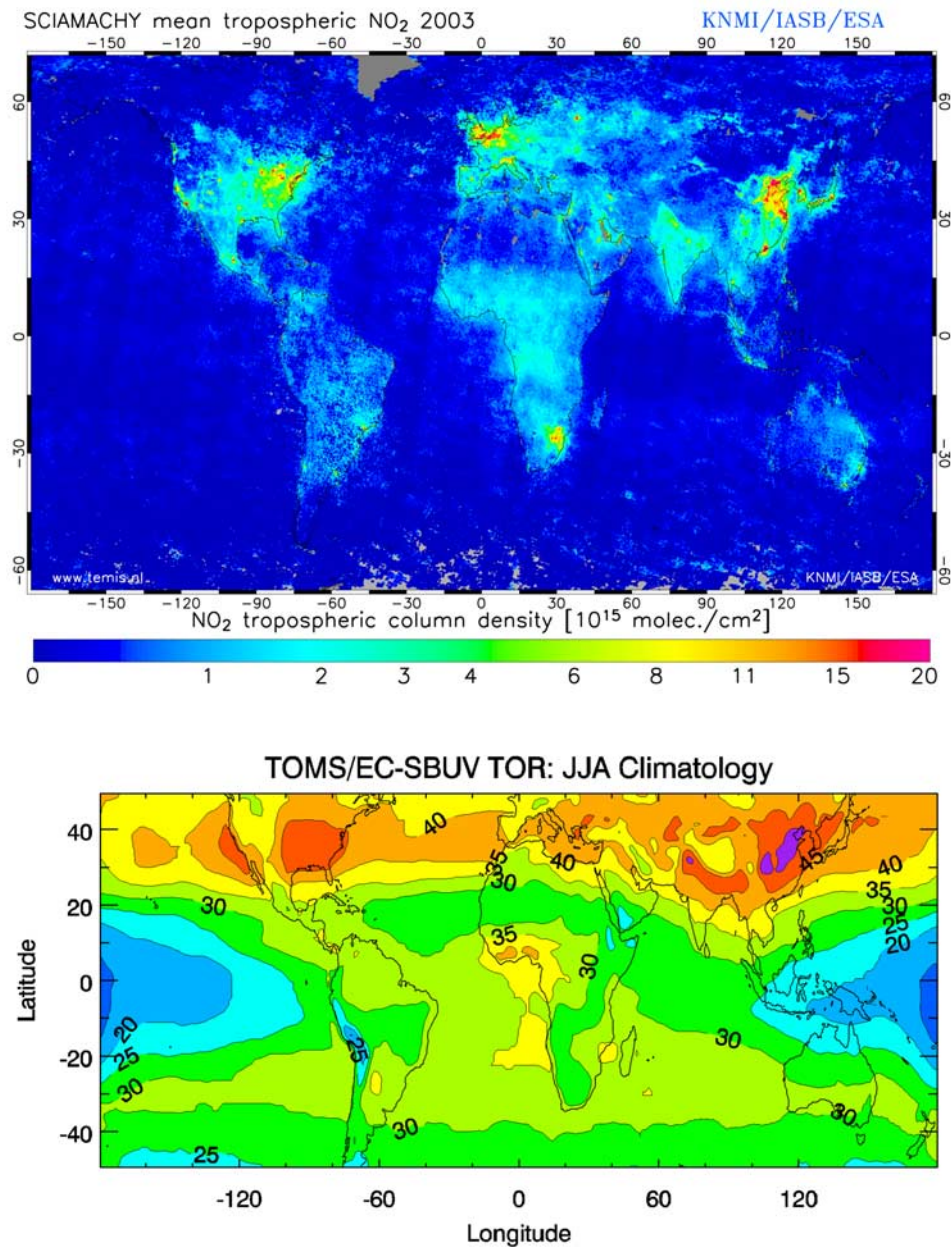


Figure 8. (top) Distribution of tropospheric NO_2 derived SCIAMACHY for the year 2003 (<http://satellite.iup.uni-heidelberg.de>). (bottom) Climatological TOR distribution during June-July-August [*Fishman et al.*, 2003].

349 Index, SOI) and found a significant statistical relationship in
 350 the TCO gradient between the two sites and the SOI. In this
 351 study, we expand on the finding first noted by *Ziemke and*
 352 *Chandra* [2003] by examining a region that is prone to
 353 pollution [*Di Girolamo et al.*, 2004] to determine whether or
 354 not the intensity of the pollution can be linked to the ENSO
 355 cycle.

356 [18] Of particular interest is the region in northern India
 357 where *Di Girolamo et al.* [2004] also observe a “pollution
 358 pool” based on aerosol optical depth measurements from
 359 4 years of Multiangle Imaging SpectroRadiometer (MISR)
 360 measurements. The amount of tropospheric ozone over this

region as well as in eastern China follows a well-defined 361
 seasonal cycle (see Table 1) with a peak in the summer, 362
 when photochemical ozone generation is highest. In addition, 363
 to this seasonal cycle, however, the Indian data suggest 364
 the interannual variability within our 1979–2000 data set is 365
 strongly correlated with the ENSO indices previously dis- 366
 cussed (see Figure 4). The correlation between the interan- 367
 nual variability of the TOR with these indices suggests a 368
 strong relationship between the ENSO and the amount of 369
 ozone pollution in northern India during the summer 370
 (Table 2). Conversely, Table 2 shows that no such relation- 371
 ship is observed over China. 372

t1.1 **Table 1.** Summary of TOR Values Over Northern India Study Region^a

t1.2	t1.3	Month	Mean TOR (DU)	Range (DU)	
				High	Low
t1.4		<i>Northern India</i>			
t1.5	January	29.9	31.6 (1998)	25.4 (1980)	
t1.6	February	29.7	33.7 (1992)	24.8 (1991)	
t1.7	March	34.7	40.4 (1989)	27.1 (1999)	
t1.8	April	44.1	47.3 (1982)	40.4 (1985)	
t1.9	May	47.4	53.0 (1982)	42.4 (1998)	
t1.10	June	48.1	52.4 (1982)	44.8 (1999)	
t1.11	July	46.5	48.5 (1982)	43.6 (1999)	
t1.12	August	42.3	44.1 (1992)	40.0 (1999)	
t1.13	September	36.9	40.3 (1990)	35.0 (1979)	
t1.14	October	32.8	34.7 (1999)	30.5 (1987)	
t1.15	November	30.5	33.3 (1981)	28.6 (1984)	
t1.16	December	27.9	29.9 (1985)	25.6 (1984)	
t1.18		<i>China</i>			
t1.19	January	27.4	30.3 (1988)	24.1 (1991)	
t1.20	February	30.4	33.9 (1990)	27.5 (1992)	
t1.21	March	34.9	39.5 (1992)	31.5 (1998)	
t1.22	April	41.3	45.1 (1984)	38.4 (1990)	
t1.23	May	45.9	49.6 (1992)	41.3 (1988)	
t1.24	June	50.7	55.4 (1979)	48.5 (1991)	
t1.25	July	50.7	53.8 (1990)	49.0 (1982)	
t1.26	August	46.8	48.6 (1999)	44.8 (1979)	
t1.27	September	40.0	41.8 (1998)	38.1 (1979)	
t1.28	October	34.5	38.6 (1998)	32.0 (1992)	
t1.29	November	31.4	33.6 (1979)	28.7 (1989)	
t1.30	December	27.9	30.6 (1982)	25.6 (1984)	

^aAll values are in Dobson Units (DU). The first column shows the average TOR by month over this region. The second and third columns show the high and low years, respectively (and the year in which these extremes occurred).

t1.31

373 [19] The significant associations shown in Table 2 also
 374 correspond with the timing of the monsoon season in this
 375 region. The monsoon season, like the TOR, exhibits con-
 376 siderable interannual variability [Krishnamurthy and
 377 Shukla, 2000; Goswami and Mohan, 2001]. Figure 9 shows
 378 a time series of the summer TOR over northern India and
 379 the SSTA in Region 4. During summers of increased TOR
 380 (1982, 1987, 1991–1992), it should be noted that there is
 381 also reduced rainfall [Parthasarathy et al., 1995]. Coinci-
 382 dently, these same years correspond to the warm phase of
 383 ENSO (i.e., “El Niño” years). A major factor contributing
 384 to monsoonal variability has been its relationship with the
 385 ENSO phenomenon. Drought years over India during the
 386 summer monsoon are often, but not exclusively, associated
 387 with warmer SSTAs in the equatorial central and eastern
 388 Pacific (El Niño) and wet years with relatively colder
 389 SSTAs (La Niña) [Rasmusson and Carpenter, 1983;
 390 Webster and Yang, 1992; Ju and Slingo, 1995]. One factor
 391 driving the monsoon-ENSO connection is the modulation in
 392 the latitudinal shift of the ITCZ exhibited during a warm
 393 phase of the preceding spring, which may be delaying the
 394 onset of the monsoon [Ju and Slingo, 1995]. The delayed
 395 northward shift in the ITCZ can affect the development of
 396 the Somali Jet and subsequent onset of the southwest
 397 monsoonal flow. This delayed onset has been shown to
 398 lead to a weakened large-scale monsoonal circulation
 399 (Somali jet) and thus a weaker monsoon overall (i.e., less
 400 precipitation) [Shukla and Wallace, 1983; Ju and Slingo,
 401 1995]. During this phase, the Walker Circulation can
 402 actually weaken or reverse itself, causing subsequent

changes in surrounding circulation regimes. Associated with
 this ITCZ shift and change in the Walker Circulation is
 increased convection over the east Pacific and increased
 subsidence over the western Pacific and east Asia. This
 increased subsidence has also been linked to a weaker
 monsoon season [Shukla and Wallace, 1983; Palmer et
 al., 1992]. Thus the relationship of increased tropospheric
 ozone to the warm phase of ENSO could be due to the
 increased subsidence over southeast Asia (analogous to
 what is observed over west Africa) and a weakened Somali
 jet, leading to a drier monsoon season. A drier monsoon
 season could lead to either increased burning or enhanced
 photochemical activity due to less cloudiness since either
 factor would lead to enhanced in situ production of tropo-
 spheric ozone [e.g., Fishman et al., 1987].

[20] Examination of the relationship between the ENSO
 cycle and the amount of ozone over China (Table 2) shows
 that there are no statistically significant correlations between
 the TOR and any monthly or seasonal SOI or SSTA regions.
 Some of the correlations are as high as 0.40 (values with
 95% confidence levels should be $\sim|0.48|$ or greater), but the
 sign of these correlations is opposite of what is seen in the
 India data.

[21] There is the possibility that increased cloud cover
 over this region during the summer monsoon period impacts

Table 2. Monthly and Seasonal Correlation Coefficients Between
 the TOR Over This Region and the SOI Index and Sea Surface
 Temperature Anomalies (SSTAs) in the ENSO SST Regions
 Shown in Figure 4^a

t1.2	Month	SOI		ENSO SST Region				t2.3
		Monthly	Seasonal	1 and 2	3	3.4	4	
t2.1	<i>India-ENSO Correlations</i>							
t2.2	January	-0.06	-0.09	0.15	0.06	0.03	0.05	t2.5
t2.3	February	-0.34	-0.48	0.12	0.28	0.34	0.23	t2.6
t2.4	March	0.03	0.02	-0.14	-0.13	-0.06	0.11	t2.7
t2.5	April	-0.15	-0.14	-0.14	0.05	0.12	0.24	t2.8
t2.6	May	0.22	0.24	-0.20	0.08	0.13	0.30	t2.9
t2.7	June	-0.43	-0.55^b	-0.11	0.27	0.41	0.44	t2.10
t2.8	July	-0.48	-0.56^b	0.06	0.40	0.59^b	0.68^c	t2.11
t2.9	August	-0.44	-0.53^b	0.12	0.45	0.57^b	0.66^c	t2.12
t2.10	September	0.13	0.19	-0.25	-0.25	-0.23	0.04	t2.13
t2.11	October	0.50^b	0.43	-0.36	-0.43	-0.47	-0.54^b	t2.14
t2.12	November	0.28	0.10	0.12	0.04	-0.01	-0.13	t2.15
t2.13	December	0.50^b	0.30	-0.02	-0.09	-0.16	-0.16	t2.16
t2.14	<i>China-ENSO Correlations</i>							
t2.15	January	-0.22	-0.14	0.12	0.15	0.17	0.19	t2.19
t2.16	February	-0.19	-0.09	0.27	0.21	0.19	0.29	t2.20
t2.17	March	-0.10	-0.01	-0.21	-0.03	0.15	0.26	t2.21
t2.18	April	-0.40	-0.38	-0.05	0.13	0.26	0.27	t2.22
t2.19	May	-0.09	-0.07	0.06	0.39	0.39	0.18	t2.23
t2.20	June	0.40	0.39	0.17	0.04	0.02	0.04	t2.24
t2.21	July	0.31	0.34	-0.38	-0.17	-0.08	-0.07	t2.25
t2.22	August	0.06	-0.16	-0.14	-0.07	-0.11	-0.19	t2.26
t2.23	September	0.20	0.21	-0.09	-0.28	-0.34	-0.35	t2.27
t2.24	October	0.31	0.29	0.16	-0.04	-0.15	-0.40	t2.28
t2.25	November	-0.04	-0.19	0.35	0.24	0.18	0.08	t2.29
t2.26	December	-0.05	-0.09	0.28	0.35	0.30	0.19	t2.30

^aThe SOI column refers to the correlation coefficient for each monthly
 TOR over the period 1979–1999 with the Southern Oscillation Index
 computed both monthly and seasonally. The last four columns show
 the correlation coefficient of the monthly TOR with the Sea Surface
 Temperature Anomalies (SSTA) calculated for the four equatorial Pacific
 regions shown in Figure 4. Significant correlations are in bold.

^bCorrelations exhibiting a 0.05 significance level.

^cCorrelations exhibiting a 0.01 significance level.

t2.31

t2.32

t2.33

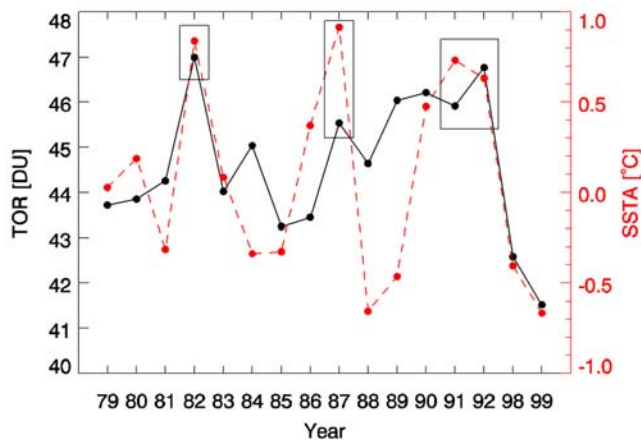


Figure 9. Relationship between summer TOR over India and ENSO Region 4 SSTAs. TOR values over northern India between 1979 and 1999 for the years that complete summertime data are available and the SSTA over the western Pacific (i.e., Region 4, see Figure 4). Blocked areas refer to strong El Niño episodes.

satellite retrievals of ozone. Generation of TOR products used in this study was derived from the TOMS archive (<http://toms.gsfc.nasa.gov/ozone/ozone.html>) which include cloudy, partially cloudy, and cloud-free pixels. When compared with TOR generated from another version of TOMS data, which allowed us to segregate individual pixels from clear and cloudy areas, the presence of clouds did not produce significant differences in the distributions derived over India and east Asia. Furthermore, validation of gradients of the type shown in this study are supported by the analysis described by *Creilson et al.* [2003], that compared spatial differences in TOR with integrated ozone derived from ozonesonde measurements.

[22] Findings from the Indian Ocean Experiment (INDOEX) confirm the hypothesis that anthropogenic emissions are responsible for the widespread presence of haze and pollution covering much of Asia and the adjacent Indian Ocean [*Lelieveld et al.*, 2001] and that such perturbations may impact the global climate system [*Ramanathan et al.*, 2001]. During the intensive field phase of INDOEX, a number of aircraft measurements found aged pollution plumes during several flights north of the Intertropical Convergence Zone (ITCZ) whose source regions were identified as northeastern India and Bangladesh [*de Gouw et al.*, 2001]. These findings are consistent with the NO_2 distribution shown in Figure 8 and with emissions data [*van Aardenne et al.*, 1999] suggesting that substantial amounts of nitrogen oxides (NO_x) should be present along the Ganges River Valley of northern India and northern Bangladesh. Because NO_x is the most important precursor for the photochemical generation of tropospheric ozone, concurrent presence of high concentrations of O_3 would not be unexpected.

5. Discussion

[23] This study has shown that IAV of ozone in both the troposphere and the stratosphere can be linked to large scale

meteorological forcing parameters associated with well-known documented phenomena: the QBO in the equatorial stratosphere and the ENSO in the tropical and subtropical troposphere. We have used monthly averaged information over a 21-year period to relate ozone to these large-scale features that have been shown to exhibit teleconnections over large parts of the globe.

[24] *Duncan et al.* [2003] have used satellite data to show that fire frequency in several regions of the world is directly tied to ENSO-induced droughts. Using Along Track Scanning Radiometer (ATSR) and TOMS Aerosol Index (AI) data, they show large enhancements in Malaysia and Indonesia in biomass burning fires and attendant widespread particulate enhancement during the El Niño periods of 1982–1983, 1991, and 1997–1998. Thus the link between ENSO and increased emissions that should lead to elevated ozone pollution concentrations has been established. Furthermore, *Di Girolamo et al.* [2003] confirm the massive amount of particulate matter present in the same region we find high TOR values in northern India. Thus, on a seasonal basis, it is fairly straightforward to link favored meteorological situations to the formation of widespread pollution.

[25] In an earlier study, *Fishman and Balok* [1999] were able to use TOR data to help interpret the development of a large air pollution episode over the eastern United States in July 1988, which was driven by the development of an unusually intense and expansive high-pressure regime over this region. Clearly, there are prevailing meteorological conditions that optimize the formation of ozone pollution on seasonal as well as on synoptic (3–7 days) timescales. In addition, *Creilson et al.* [2003] have used the IAV of this TOR data set to show a relationship between transcontinental transport and the North Atlantic Oscillation (NAO). The ultimate goal of these kinds of studies is to establish a means of linking specific meteorological situations to the potential onset of elevated ozone periods. This study suggests that such relationships can be done in some regions (west Africa and northern India) in a statistical seasonal sense. *Fishman and Balok* showed that certain meteorological conditions are conducive to ozone formation on shorter timescales that are even more intense and it is these specific intense episodes that lead to the most pronounced damage to plants, crops, and human health [*Chameides et al.*, 1999; *Cheung and Wang*, 2001]. If we can understand such relationships, and then forecast them correctly in pure meteorological terms, then perhaps we can mitigate the impact of the formation of ozone by reducing regional emissions. As shown by *Bell et al.* [2004], the reduction of surface ozone concentrations by only as little as 10 ppbv could result in lowering premature deaths by several thousand per year in the United States. Extrapolation of such reductions of exposure to high concentrations worldwide would have an enormous benefit that would be difficult to quantify.

6. Summary and Conclusions

[26] We have presented an analysis of interannual variability using a data set that spans more than two decades. This analysis shows that the methodology used to separate the troposphere from the stratosphere in these concurrent measurements from TOMS and SBUV instruments produces

two long-term records that are independent of each other. Our analysis of the IAV of the SCO data reproduces previous findings using TOMS total ozone and SAGE stratospheric ozone profile measurements that show that the amount of stratospheric ozone at low latitudes is highly linked to meteorological processes that drive the QBO. On the other hand, there is a much weaker relationship between the TOR product derived from these same satellite measurements and the QBO. At the same time, we have shown that there is a strong correlation between TOR and ENSO during specific times of the year, but only at specific much smaller scale regimes. The months that favor enhanced levels of tropospheric ozone are consistent with our understanding from a meteorological point of view as to why higher ozone values should be produced; i.e., at times when subsidence is more prevalent and when local precipitation is suppressed.

[27] In recent years, the development of air quality models for understanding the formation of ozone episodes has accelerated with the intent of becoming operational in less than a decade [Dabberdt et al., 2004]. This study, on the other hand, has used historical measurements in an attempt to identify what meteorological regimes have been most conducive to widespread ozone formation on a monthly basis. Relating these monthly distributions to prevailing meteorological conditions will hopefully provide insight into analogous ozone-producing events on smaller timescales that lead to prolonged elevated ozone events providing the eventual capability of relating these situations to what is observed at the surface, as was done by Fishman and Balok [1999]. The first use of satellite information being used in near-real-time to improve air-quality forecasts has recently been demonstrated [Szykman et al., 2004; Al-Saadi et al., 2005] with the goal to use such forecasts to warn the public so that they can take measures to reduce exposure to high pollutant concentrations as well as to reduce emissions in specific regions so that less ozone is actually produced. Achieving an understanding between meteorology, satellite measurements representative of tropospheric pollution, and high concentrations at the ground is long-term goal of this research [Fishman et al., 2005] and clearly beyond the scope of the present study. However, we feel that this study has succeeded in showing that regional TOR distributions are influenced by prevailing meteorological conditions related to large-scale weather patterns and that this is the first step in attempting to forecast high tropospheric ozone levels on shorter timescales. In turn, using such information in a short-term predictive mode can mitigate the pollution's detrimental effects on human health.

[28] This study has used satellite data from two satellites originally designed in the 1970s that had not been intended to derive any information about tropospheric ozone. With the launch of the ESA's (European Space Agency) Envisat in 2002 and NASA's (National Aeronautics and Space Agency) Aura in 2004, new generations of instruments are measuring ozone and ozone pollution precursors with capabilities that provide much better resolution and accuracy. As the data from these satellites become available to the scientific community, we expect to glean even more insight into how regional and global pollution patterns evolve and how such patterns are related to prevailing meteorological conditions. Last, as these new measurements become available from these satellites, the data described in

this study can also be used as a benchmark to quantify how atmospheric composition has been modified over decadal timescales.

[29] **Acknowledgment.** We appreciate comments on earlier versions of this paper from J. Ziemke, S. Chandra, and P. Bhartia, NASA Goddard Space Flight Center; M. Newchurch, University of Alabama-Huntsville; J. Lelieveld and M. Lawrence, Max-Planck-Institute for Chemistry; and V. Ramanathan, Scripps Institute of Oceanography.

References

- Al-Saadi, J., et al. (2005), Improving national air quality forecasts with satellite aerosol observations, *Bull. Am. Meteorol. Soc.*, in press.
- Bell, M. L., A. McDermott, S. L. Zeger, J. M. Samet, and F. Dominici (2004), Ozone and short-term mortality in 95 U.S. urban communities, *J. Am. Med. Assoc.*, 292(19), 2372–2378.
- Bowman, K. P. (1989), Global patterns of the quasi-biennial oscillation in total ozone, *J. Atmos. Sci.*, 46, 3328–3343.
- Chameides, W. L., et al. (1999), Is ozone pollution affecting crop yields in China, *Geophys. Res. Lett.*, 26, 867–870.
- Chandra, S., and R. S. Stolarski (1991), Recent trends in stratospheric total ozone: Implications of dynamical and El Chichon perturbations, *Geophys. Res. Lett.*, 18, 227–2280.
- Cheung, V. T. F., and T. Wang (2001), Observational study of ozone pollution at a rural site in the Yangtze Delta of China, *Atmos. Environ.*, 35, 4947–4958.
- Cook, K. H. (1999), Generation of the African easterly jet and its role in determining West African precipitation, *J. Clim.*, 12, 1165–1184.
- Creilson, J. K., J. Fishman, and A. E. Wozniak (2003), Intercontinental transport of tropospheric ozone: A study of its seasonal variability across the North Atlantic and its relationship to the North Atlantic Oscillation, *Atmos. Chem. Phys.*, 3, 2053–2066.
- Dabberdt, W. F., et al. (2004), Meteorological research needs for improved air quality forecasting: Report of the 11th Prospectus Development Team of the U.S. Weather Research Program, *Bull. Am. Meteorol. Soc.*, 85, 563–586.
- de Gouw, J. A., et al. (2001), Overview of the trace gas measurements on board the Citation aircraft during the intensive field phase of INDOEX, *J. Geophys. Res.*, 106, 28,453–28,468.
- Di Girolamo, L., et al. (2004), Analysis of Multi-angle Imaging Spectro-Radiometer (MISR) aerosol optical depths over greater India during winter 2001–2004, *Geophys. Res. Lett.*, 31, L23115, doi:10.1029/2004GL021273.
- Duncan, B. N., R. V. Martin, A. C. Staudt, R. Yevich, and J. A. Logan (2003), Interannual and seasonal variability of biomass burning emissions constrained by satellite observations, *J. Geophys. Res.*, 108(D2), 4100, doi:10.1029/2002JD002378.
- Edwards, D. P., et al. (2003), Tropospheric ozone over the tropical Atlantic: A satellite perspective, *J. Geophys. Res.*, 108(D8), 4237, doi:10.1029/2002JD002927.
- Fishman, J., and A. E. Balok (1999), Calculation of daily tropospheric ozone residuals using TOMS and empirically improved SBUV measurements, *J. Geophys. Res.*, 104, 30,319–30,340.
- Fishman, J., F. M. Vukovich, D. R. Cahoon, and M. C. Shipham (1987), The characterization of an air pollution episode using satellite total ozone measurements, *J. Clim. Appl. Meteorol.*, 26, 1638–1654.
- Fishman, J., A. E. Wozniak, and J. K. Creilson (2003), Global distribution of tropospheric ozone from satellite measurements using the empirically corrected tropospheric ozone residual technique: Identification of the regional aspects of air pollution, *Atmos. Chem. Phys.*, 3, 893–907.
- Fishman, J., D. P. McNamara, J. J. Szykman, A. E. Wozniak, and J. K. Creilson (2005), An exploratory study to use OMI total ozone data in near-real-time to produce a guidance product or air quality forecasters, paper presented at EOS Aura Science Team Meeting, Natl. Aeronaut. and Space Admin., Pasadena, Calif.
- Frankenberg, C., U. Platt, and T. Wagner (2005), Retrieval of CO from SCIAMACHY onboard ENVISAT: Detection of strongly polluted areas and seasonal patterns in global CO abundances, *Atmos. Chem. Phys.*, 5, 1639–1644.
- Goswami, B. N., and R. S. A. Mohan (2001), Intraseasonal oscillations and interannual variability of the Indian summer monsoon, *J. Clim.*, 14, 1180–1198.
- Grist, J. P., and S. E. Nicholson (2001), A study of the dynamic factors influencing the rainfall variability in the west African Sahel, *J. Clim.*, 14, 1337–1359.
- Hasebe, F. (1996), Quasi-biennial oscillations of ozone and diabatic circulation in the equatorial stratosphere, *J. Atmos. Sci.*, 51, 729–745.

- 661 Heck, W. H., R. M. Adams, W. W. Cure, A. S. Hoagle, H. E. Heggestad,
662 R. Kohut, L. W. Kress, J. O. Rawlings, and O. C. Taylor (1983), A reassess-
663 ment of crop loss from ozone, *Environ. Sci. Technol.*, *17*, 573A–581A.
- 664 Ju, J., and J. Slingo (1995), The Asian summer monsoon and ENSO, *Q. J. R. Meteorol. Soc.*, *121*, 1133–1168.
- 666 Kalnay, E., et al. (1996), The NCEP/NCAR Reanalysis 40-year Project,
667 *Bull. Am. Meteorol. Soc.*, *77*, 437–471.
- 668 Kinnersley, J. S., and K.-K. Tung (1998), Modeling the global interannual
669 variability of ozone due to the equatorial QBO and to extratropical
670 planetary wave variability, *J. Atmos. Sci.*, *55*, 1417–1428.
- 671 Koren, H. S., et al. (1989), Ozone-induced inflammation in the lower
672 airways of human subjects, *Am. Rev. Respir. Dis.*, *139*, 407–415.
- 673 Krishnamurthy, V., and J. Shukla (2000), Intraseasonal and interannual
674 variability of rainfall over India, *J. Clim.*, *13*, 4366–4377.
- 675 Lelieveld, J., et al. (2001), The Indian Ocean experiment: Widespread air
676 pollution from South and Southeast Asia, *Science*, *291*, 1031–1036.
- 677 Lindzen, R. S., and J. R. Holton (1968), A theory of the quasi-biennial
678 oscillation, *J. Atmos. Sci.*, *25*, 1095–1107.
- 679 Lippmann, M., and R. B. Schlessinger (2000), Toxicological bases for the
680 setting of health-related pollution standards, *Annu. Rev. Public Health*,
681 *21*, 309–333.
- 682 Logan, J. A. (1999), An analysis of ozonesonde data for the troposphere:
683 Recommendations for testing 3-D models, and development of a gridded
684 climatology for tropospheric ozone, *J. Geophys. Res.*, *104*, 16,115–
685 16,149.
- 686 Nicholson, S. E., and J. P. Grist (2003), The seasonal evolution of the
687 atmospheric circulation over West Africa and equatorial Africa, *J. Clim.*,
688 *16*, 1013–1030.
- 689 Nicholson, S. E., and J. Kim (1997), The relationship of the El Niño-
690 Southern Oscillation to African rainfall, *Int. J. Climatol.*, *17*, 117–135.
- 691 Palmer, T. N., C. Brankovic, P. Viterbo, and M. J. Miller (1992), Modeling
692 interannual variations of summer monsoons, *J. Clim.*, *5*, 399–417.
- 693 Parthasarathy, B., A. A. Munot, and D. R. Kothawale (1995), Monthly and
694 seasonal rainfall series for all-India homogeneous regions and meteorolo-
695 gical subdivisions: 1871–1994, *Res. Rep. RR-065*, Ind. Inst. of Trop.
696 Meteorol., Pune, India.
- 697 Philander, S. G. H. (1990), *El Niño, La Niña, and the Southern Oscillation*,
698 *Int. Geophys. Ser.*, vol. 46, 289 pp., Elsevier, New York.
- 699 Ramanathan, V., et al. (2001), Indian Ocean experiment: An integrated
700 analysis of the climate forcing and effects of the great Indo-Asian haze,
701 *J. Geophys. Res.*, *106*, 28,371–28,398.
- 702 Randel, W. J., and F. Wu (1996), Isolation of ozone QBO in SAGE II data
703 by singular-value decomposition, *J. Atmos. Sci.*, *53*, 2546–2559.
- 704 Rasmusson, E. M., and T. H. Carpenter (1983), The relationship between
705 eastern equatorial Pacific sea surface temperatures and rainfall over India
706 and Sri Lanka, *Mon. Weather Rev.*, *111*, 517–528.
- 707 Reed, R. J. (1965), The quasi-biennial oscillation of the atmosphere be-
708 tween 30 and 50 km over Ascension Island, *J. Atmos. Sci.*, *22*, 331–333.
- Shukla, J., and J. M. Wallace (1983), Numerical simulation of the atmo- 709
spheric response to equatorial Pacific sea surface temperature anomalies, 710
J. Atmos. Sci., *40*, 1613–1630. 711
- Skelly, J. M. (2000), Tropospheric ozone and its importance to forests and 712
natural plant communities of the northeastern United States, *Northeast* 713
Nat., *3*, 221–236. 714
- Spektor, D. M., M. Lippmann, P. J. Lioy, G. D. Thurston, K. Citak, D. J. 715
James, N. Bock, F. E. Speizer, and C. Hayes (1988), Effects of ambient 716
ozone on respiratory function in active, normal children, *Am. Rev. Respir.* 717
Dis., *137*, 313–320. 718
- Staehelin, J., J. Thudium, R. Buhler, A. Volz-Thomas, and W. Gräber 719
(1994), Trends in surface ozone concentrations at Arosa (Switzerland), 720
Atmos. Environ., *28*, 75–87. 721
- Szykman, J., J. White, R. Pierce, J. Al-Saadi, D. Neil, C. Kittaka, D. Chu, 722
L. Remer, L. Gumley, and E. Pjris (2004), Utilizing MODIS satellite 723
observations in near-real-time to improve AIRNOW next day forecast of 724
fine particulate matter, paper presented at Sixth Conference on Atmo- 725
spheric Chemistry, Am. Meteorol. Soc., Seattle, Wash. 726
- Torres, O., and P. K. Bhartia (1999), Impact of tropospheric aerosol absorp- 727
tion on ozone retrieval from backscattered ultraviolet measurements, 728
J. Geophys. Res., *104*, 21,569–21,577. 729
- Tung, K.-K., and H. Yang (1994), Global QBO in circulation and ozone: 730
Part I. Reexamination of observational evidence, *J. Atmos. Sci.*, *51*, 731
2699–2707. 732
- van Aardenne, J. A., G. R. Carmichael, H. Levy II, D. Streets, and 733
L. Hordijk (1999), Anthropogenic NO_x emissions in Asia in the 734
period 1990–2020, *Atmos. Environ.*, *33*, 633–646. 735
- Volz, A., and D. Kley (1988), Evaluation of the Montsouris series of ozone 736
measurements made in the nineteenth century, *Nature*, *332*, 240–242. 737
- Webster, P. J., and S. Yang (1992), Monsoon and ENSO: Selectively inter- 738
active systems, *Q. J. R. Meteorol. Soc.*, *118*, 877–926. 739
- Wozniak, A. E., J. Fishman, P.-H. Wang, and J. K. Creilson (2005), Dis- 740
tribution of stratospheric column ozone (SCO) determined from satellite 741
observations: Validation of solar backscatter ultraviolet (SBUV) measure- 742
ments in support of the tropospheric ozone residual (TOR) method, 743
J. Geophys. Res., in press. 744
- Ziemke, J. R., and S. Chandra (2003), La Niña and El Niño–induced 745
variabilities of ozone in the tropical lower atmosphere during 1970– 746
2001, *Geophys. Res. Lett.*, *30*(3), 1142, doi:10.1029/2002GL016387. 747
- J. K. Creilson, J. Fishman, and A. E. Wozniak, NASA Langley Research 749
Center, Mail Stop 401A, Hampton, VA 23681, USA. (j.k.creilson@larc. 750
nasa.gov; jack.fishman@nasa.gov; a.e.wozniak@larc.nasa.gov) 751
- P. J. Crutzen, Max-Planck-Institute for Chemistry, P.O. Box 3060, Mainz, 752
Germany, D-55020. (air@mpch-mainz.mpg.de) 753